ELSEVIER

Polymer 40 (1999) 3413–3420

polymer

Pyroelectric properties and dielectric hysteresis of a poly(vinyl alcohol) with azobenzene-alkoxy side chains

P. Frübing*, M. Wegener, R. Gerhard-Multhaupt, A. Buchsteiner, W. Neumann, L. Brehmer

Department of Physics, University of Potsdam, Am Neuen Palais 10, D-14469 Potsdam, Germany

Received 1 May 1998; received in revised form 26 June 1998; accepted 14 July 1998

Abstract

After thermal poling, pyroelectricity and a pronounced dielectric hysteresis have been observed on films of a poly(vinyl alcohol) with azobenzene-alkoxy side chains (Az-PVA). Based on dielectric spectroscopy data and structural information from differential thermal analysis, the pyroelectricity can be explained with reversible dipole–density changes during thermal expansion, whereas the dielectric hysteresis is proposed to result from the polarisation caused by charge carriers, probably ions. These findings are also significant for the interpretation of dielectric hysteresis measurements on other polymer-electret materials. © 1999 Elsevier Science Ltd. All rights reserved.

Keywords: Poly(vinyl alcohol); Azobenzene group; Side-chain polymer

1. Introduction

Pyroelectricity in polymers with oriented molecular dipoles has been investigated for more than 20 years. In these studies, relaxation processes and the nondestructive probing of spatial polarisation distributions were of particular interest (see e.g. Bauer [1]). Furthermore, pyroelectric films of PVDF and PVDF-TrFE have been successfully employed in infrared detectors and other device applications; pertinent reviews were provided by Xiao and Lang [2] and Coufal and Mandelis [3]. Recent developments in the field of pyroelectric polymers and their applications have been reviewed by Bauer and Lang [4] and by Bauer [5].

Polymers with azobenzene-containing side chains have attracted considerable interest as candidates for nonlinear optical applications [6]. Together with donor and acceptor groups that are linked by its delocalised π-electron system, the azobenzene group forms a strong dipole (A-π-D dipole). The known aggregation tendency of azo-chromophores may lead to the formation of dipolar domains with enhanced dipole moment. Therefore, azobenzene-containing polymers are interesting materials also for pyroelectrical investigations. However, the microscopic processes which cause the pyroelectric activity in polymers depend strongly on chemical structure, molecular conformation and morphology. Pyroelectricity may arise from the libration of molecular dipoles or dipolar domains and from dipole-density changes during thermally induced expansion or contraction of the material. In semi-crystalline polymers, reversible changes of crystallinity as well as trapped charge carriers may also contribute to the pyroelectricity [7].

We studied a side-chain polymer based on a poly(vinyl alcohol) with azobenzene-alkoxy side groups. Together with oxygen as electron donor and the carboxyl group as electron acceptor, the azobenzene unit forms an A-π-D-dipole. Our aim was to investigate the contributions of the A-π-D-dipoles to electric polarisation and to pyroelectricity. To this end, we determined the pyroelectric coefficient as well as the polarisation charge and its temperature and frequency dependencies by means of quasi-static pyroelectric measurements [8], dielectric hysteresis experiments, and dielectric spectroscopy, respectively. We interpret the results with the help of micro-structural information mainly obtained from differential scanning calorimetry. A combination of dielectric spectroscopy and thermal analysis has been already successfully employed in similar investigations of other polymers containing strong molecular dipoles [9,10].

* Corresponding author. Tel.: +49-331-9771456; Fax: +49-331-9771490; E-mail: fruebing@rz.uni-potsdam.de

PII: S0032-3861(98)00563-1

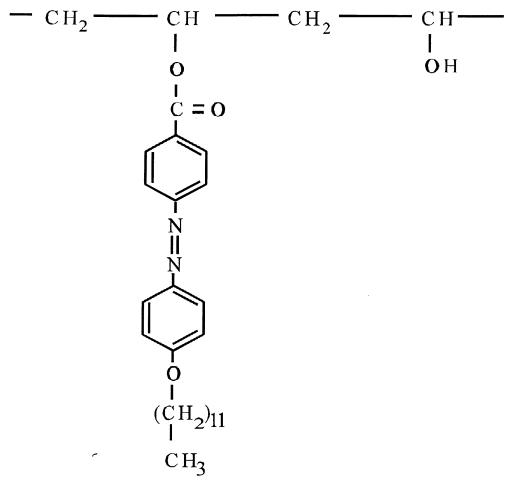

Fig. 1. Chemical structure of Poly[(vinyl-4′-n-dodecyloxyazobenzene-4-carboxylate)-co-(vinyl alcohol) 1:1] (Az-PVA).

2. Sample material

Poly[(vinyl-4′-n-dodecyloxyazobenzene-4-carboxylate)-co-(vinyl alcohol) 1:1] (Az-PVA) (Fig. 1) has been synthesised by Einhorn esterification of a commercial poly(vinyl alcohol) (molecular mass 72 000 g mol^{-1}, degree of polymerisation 1600) and 4′-n-dodecyloxyazobenzene-4-carboxylic acid [11].

The maximum degree of esterification is 85%, as calculated from elemental analysis. The azobenzene-alkoxy side chains are statistically distributed. Without excitation, the azobenzene A-π-D dipoles generally assume the trans (E) conformation. The dipole moments of the E and Z conformations of the dipolar unit are 4.9 and 2.4 D, respectively. They were calculated by means of a restricted Hartree–Fock method, using the semi-empirical molecular orbital package (MOPAC) version 6.0 with the Austin model (AM1) Hamiltonian. The mean error of the dipole moments calculated with this method is 0.4 D [12].

The melting point, as determined with differential scanning calorimetry (DSC) on powder is 197°C. The loss of mass, measured by means of thermogravimetric analysis (TGA), is approx. 1% up to 160°C and increases to approx. 1.5% up to the melting point. A pronounced thermal degradation takes place at temperatures above 280°C. The thermal stability of the material was also checked with infrared spectroscopy. In the infrared spectrum, after annealing of the material in air at 180°C for 20 min, there is no indication of any changes in the chemical composition.

3. Experimental details

3.1. Sample preparation

The samples were obtained by casting a 2% chloroform solution of the Az-PVA on aluminium-coated glass or stainless-steel substrates. Free-standing films were prepared by coating the solution on a Teflon plate and separating the dried solid film from the plate by means of submersion into distilled water. The as-prepared films are transparent and reddish coloured. The thickness of the films was roughly determined by means of weighing assuming a density of 1.0 g cm^{-3}. In addition, the thickness was checked with a laser displacement meter based on triangulation (Keyence LD-2500). The thickness data are accurate within ± 20%.

3.2. Differential scanning calorimetry (DSC)

DSC measurements on the Az-PVA films were performed with a Perkin–Elmer DSC 7 in the temperature range from 10 to 210°C. The heating and cooling rates were 20 K min^{-1}.

3.3. Thermal poling

Since the as-prepared polymer is isotropic, a preferential dipole orientation and thus also pyroelectricity was achieved by means of thermal poling. A dc field of at most 75 MV m^{-1} was applied vertically to the plane of the film at 180°C for 30 min. Subsequently, the samples were cooled to room temperature under the field with a rate of − 5 K min^{-1}. Thermal poling was performed under dry nitrogen atmosphere.

3.4. Pyroelectric measurements

Pyroelectricity is the reversible change of the spontaneous or induced polarisation P with temperature. If a pyroelectric material, sandwiched between metal electrodes and shorted through a sensitive electrometer, is exposed to a slow sinusoidal temperature oscillation, the pyroelectric current I_P is given by:

$$I_p = Ap(T)\omega T_0 \cos(\omega t) \quad (1)$$

where T_0 is the amplitude and ω the angular frequency of the temperature oscillation, A is the electrode area and $p = dP/dT$ is the pyroelectric coefficient. The measurement of this current is known as the quasistatic pyroelectric method [8]. It should be noted that in reality, the temperature derivative $p_{exp} = (1/A)(dQ/dT)$ of charge Q induced on the sample electrodes is detected and that the electrode area is presumed to be temperature independent.

Nonpyroelectric current contributions can be eliminated on the basis of the phase shift between total current and temperature. The pyroelectric coefficient is then calculated from the amplitude of the pyroelectric current according to Eq. (1).

Typical experimental parameters were a modulation frequency of $f = 6.7$ mHz, a modulation amplitude of $T_0 = 1.0$ K and a mean temperature of $T = 25.0$°C. The sinusoidal temperature variation was achieved with a flow of cooled nitrogen gas and a fast heater, both controlled with the Novocontrol Cryosystem Quatro. The current was measured

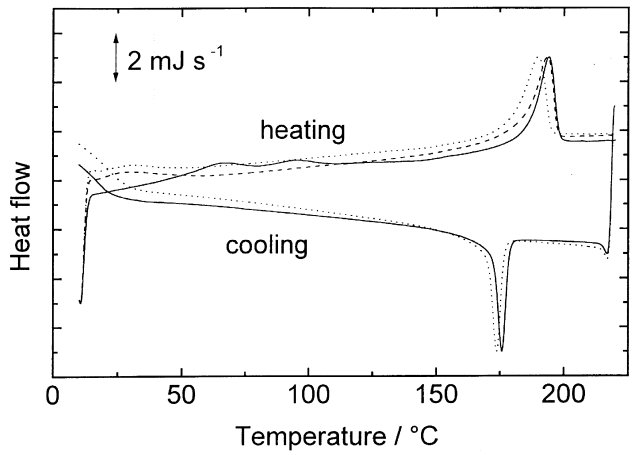

Fig. 2. DSC thermogram of the Az-PVA film; ——, first cycle; - - -, second cycle; · · ·, third cycle. After the second heating, the sample was rapidly cooled down to liquid nitrogen temperature.

with a Keithley 617 electrometer. Further experimental details are reported elsewhere [13]. In general, the measurements were carried out on 2.0-μm thick films deposited on aluminium-coated glass plates and coated with a rectangular aluminium top electrode (electrode area (8 ± 0.5) mm^2).

3.5. Dielectric hysteresis measurements

A polarising field, sinusoidally varying at a frequency of 3.0 mHz, was applied to the sample by means of a bipolar high-voltage power supply (FUG HCB 6500) whose output was controlled with a waveform generator. The current response was measured with a HP 3458A multimeter in the current mode on free-standing films (20 μm-thick) with evaporated circular aluminium contacts (area (1.00 ± 0.01) cm^2). For the experiment, the samples were pressed between disc-shaped nickel–silver electrodes. The temperature was adjusted by heating the whole arrangement in a dry nitrogen atmosphere and was kept constant within ± 0.5 K during each measurement.

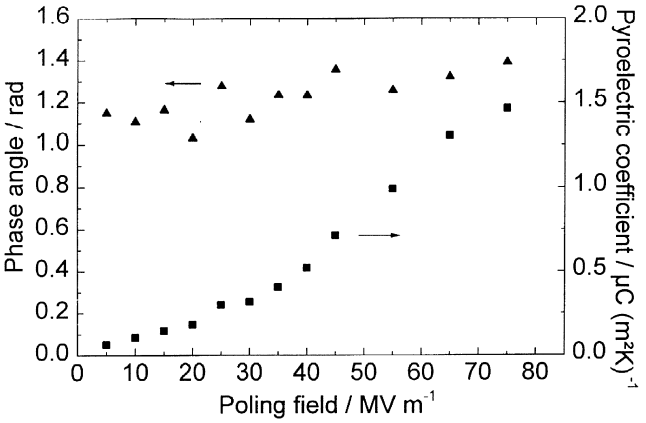

Fig. 3. Poling field dependences of the phase-angle difference between total current and temperature, as well as of the pyroelectric coefficient at room temperature; poling parameters: $T_{Pol} = 180$°C and $t_{Pol} = 30$ min; parameters of the sinusoidal temperature variation: $f = 6.7$ mHz and $T_1 = 1.0$ K.

3.6. Dielectric spectroscopy

Frequency-domain dielectric spectroscopy was carried out in a frequency range from 32 mHz to 100 kHz and in a temperature range between −105 and +155°C (first series of measurements) and from 3 mHz to 300 kHz between 120 and 180°C (second series of measurements) with a Schlumberger 1260 impedance analyser and a Chelsea dielectric interface. The samples were heated in a nitrogen gas stream by use of the Novocontrol Cryosystem Quatro. During a measurement, the temperature was kept constant within ± 0.1 K. The measurements were performed on free-standing films (thickness 20 μm) pressed between disc-shaped gold electrodes (area (7.07 ± 0.01) cm^2).

4. Results and discussion

4.1. Thermal analysis

A typical DSC thermogram (three runs) of the film is shown in Fig. 2. After the second heating run, the sample was rapidly cooled with liquid nitrogen. Apart from the melting and crystallisation peaks, the temperature-dependent variations of the specific heat are small. The latent heats for melting and crystallisation are almost equal and do not change significantly upon repeated heating and cooling. After the first melting, the features at temperatures below the melting peak that are visible in the first heating run disappear. The heat of crystallisation is approximately 11 J g^{-1}. A comparison to the corresponding value of 140 J g^{-1} for poly(ethylene terephthalate) with 35% crystallinity [14] indicates that the crystallinity of the present material is low. A distinct glass transition was not found. Therefore, it is assumed that the amorphous part of the film material remains in the glassy state until the melting region is reached.

4.2. Electrical and pyroelectrical measurements

From current–voltage characteristics, the dc conductivity of the films was found to be between 10^{-14} and 10^{-13} S m^{-1} at room temperature. The conduction current is thermally activated with an activation energy of (0.86 ± 0.09) eV, determined in the temperature range of 60–180°C. At elevated temperatures, it is influenced by the annealing process which leads to considerably lower currents and probably also to higher activation energies. Up to now, these features have not been investigated in detail.

In Fig. 3, the pyroelectric coefficient and its phase angle are presented as functions of the poling field. The poling-field dependence of the pyroelectric coefficient deviates from the expected behaviour of amorphous glassy polymers. As proposed by Mopsik and Broadhurst [15], the pyroelectric activity of such polymers is mainly caused by dipole-density changes upon thermal expansion and contraction. In this case, proportionality between the pyroelectric

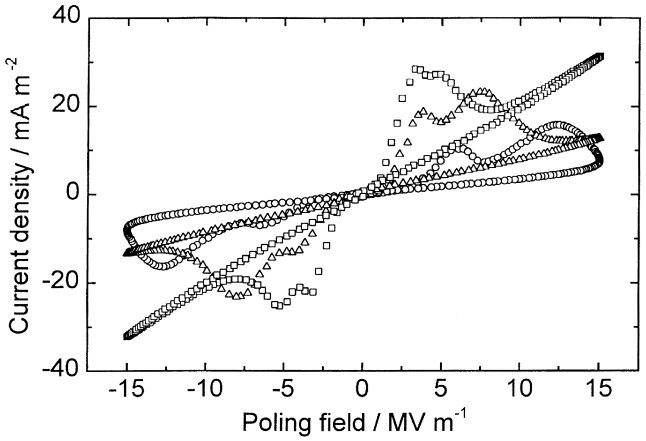

Fig. 4. Bipolar current–voltage loops at different temperatures; ○, 120°C; △, 140°C; □, 160°C.

coefficient and polarisation can be expected. The polarisation, and thus also the pyroelectric coefficient should follow the Langevin function. Experimentally, the pyroelectric coefficient tends to saturate at high fields, but there are marked deviations from the expected slope at low fields.

The time stability of the pyroelectric response in the same material was investigated by Brehmer et al. [16]. At room temperature, no significant decrease of the pyroelectric activity was observed over a period of 300 days.

4.3. Dielectric hysteresis measurements

Since Az-PVA contains strong molecular dipoles, it should be examined whether it exhibits ferroelectric hysteresis behaviour in the sense that the cooperative reorientation of ordered dipoles is only possible above a certain electric field strength and that there is a remanent polarisation at zero field.

The hysteresis measurements were performed at several temperatures. Fig. 4 shows typical current–voltage loops

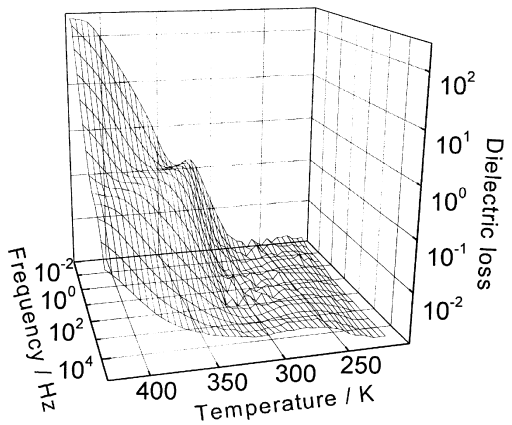

Fig. 5. Dielectric loss spectrum of Az-PVA; frequency range 32 mHz to 100 kHz, temperature range −105 to +155°C.

obtained with a sinusoidally varying voltage at the temperatures indicated. No hysteresis loop has been observed below 80°C within the ranges of cycling frequency and electric field possible without electrical breakdown.

It is obvious that two distinct polarisation processes contribute to the observed current. Furthermore, the capacitive contribution is negligible and the conduction is ohmic as long as the field is not too high. The conductivities determined from the ohmic part of the conduction currents agree very well with the values calculated from the conductivity parameters given above. Therefore, it makes sense to separate the contributions of the induced polarisation processes from the capacitive and conduction components. The saturation polarisation at temperatures above 120°C is then determined to be between 0.2 and 0.3 C m^{-2}.

Using the Onsager cavity model, Mopsik and Broadhurst [15] derived an equation for the total polarisation P in an electret material with molecular dipoles:

$$P = \frac{\varepsilon_\infty + 2}{3} N_D \mu \langle \cos\Theta \rangle \quad (2)$$

where ε_∞ is the unrelaxed relative permittivity of the sample material, N_D the dipole concentration, μ the permanent dipole moment, and $< \cos \Theta >$ is the average tilt of the dipole moments. With this equation, the maximum dipolar polarisation P_S (all dipoles are fully aligned along the field direction) can be estimated from the number densities and the effective dipole moments of the intrinsic dipolar groups. It is assumed that the polarisation stems mainly from the A-π-D dipoles and from hydroxyl groups, therefore:

$$P = \frac{\varepsilon_\infty + 2}{3} (N_{OH}\,\mu_{OH} + N_{A\text{-}\pi\text{-}D}\,\mu_{A\text{-}\pi\text{-}D}) \quad (3)$$

where N_{OH} and $N_{A\text{-}\pi\text{-}D}$ are the dipole number densities and μ_{OH} and $\mu_{A\text{-}\pi\text{-}D}$ the dipole moments of the OH and A-π-D dipoles, respectively. The dipole concentrations are calculated from molecular mass, degree of esterification and sample density (1.0 g cm^{-3}). The dipole moment of the A-π-D dipoles in their trans conformation has been calculated with molecular modelling as $\mu_{A\text{-}\pi\text{-}D} = 4.9$ D (see above). For the OH group, a dipole moment of $\mu_{OH} = 1.67$ D is found in the literature [17]. With $\varepsilon_\infty = 1.8$ (see below), $N_{OH} = 2.40 \times 10^{26}$ m^{-3} and $N_{A\text{-}\pi\text{-}D} = 1.36 \times 10^{27}$ m^{-3}, a maximum polarisation of $P_S = 3.0 \times 10^{-2}$ C m^{-2} is calculated, which is about one order of magnitude smaller than the experimentally determined values such as e.g. 0.27 C m^{-2} at 140°C.

This discrepancy clearly shows that processes of dipolar origin cannot be the main cause of the large polarisation measured. The large experimental polarisation values can only be understood as an effect of charge accumulation at internal boundaries. It should be noted that the current saturates already at relatively low fields of approx. 10 MV m^{-1}, whereas a dipolar current would usually saturate at much higher fields. The same argument applies in a reverse manner to the field dependence of the pyroelectric coefficient

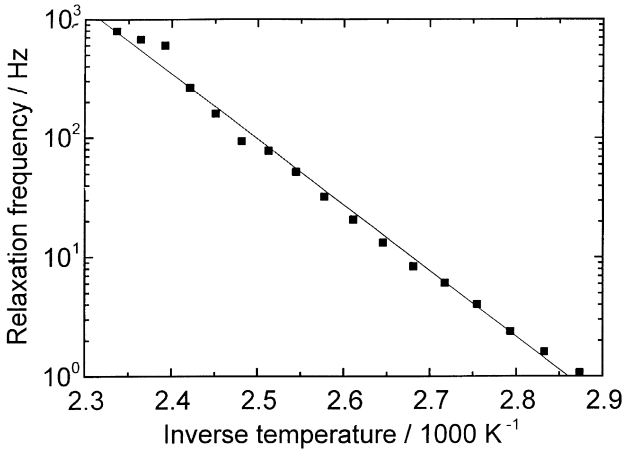

Fig. 6. Arrhenius plot for the high-frequency relaxation; ———, linear regression, correlation factor 0.998.

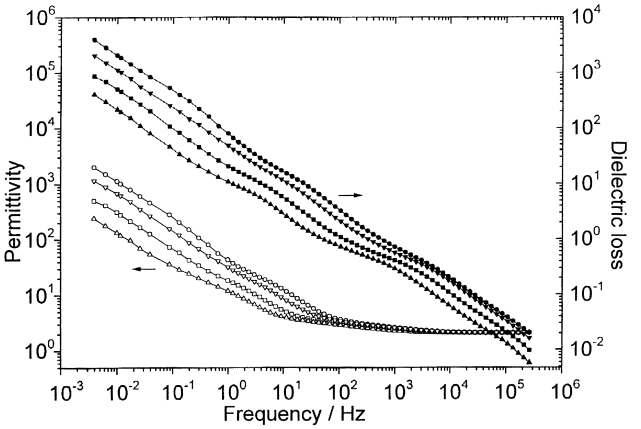

Fig. 7. Real and imaginary parts of the complex permittivity vs frequency at different temperatures; △,▲, 120°C; □,■, 140°C; ▽,▼, 160°C; ○,●, 180°C.

(Fig. 3). Therefore, it can be concluded that the pyroelectric effect in the sample material is not related to the main component of the polarisation observed in the hysteresis measurements.

An ionic polarisation charge seems to be more likely than an electronic one. The current–voltage traces of Fig. 4 are practically independent of polarity which means that the polarisation charge is intrinsic and that injection can be excluded. From a chemical point of view, it is possible that the sample material contains large ions. The salt pyridinium hydrochloride is formed during the esterification process. It is difficult to remove this salt completely [18].

Dielectric hysteresis curves with remanent polarisation values of the same order as in our experiments were found also by Fukada et al. [19] and by Hattori et al. [20] in polyureas and were attributed to ionic impurities.

4.4. Dielectric spectroscopy

An overview of the dielectric loss spectrum (temperature range from − 105 to 155°C, frequency range from 32 mHz to 100 kHz) is shown in Fig. 5. Below room temperature, the dielectric loss ε'' is rather low. There is only a flat dispersion with $\varepsilon''_{max} \approx 0.002$. At room temperature, a permittivity ε' of 1.8 is measured over almost the whole frequency range (not shown). Above room temperature, two relaxation regions are visible in Fig. 5: a 'low-frequency' and a 'high-frequency' relaxation. However, the low-frequency relaxation appears only as a shoulder at the highest temperatures and lowest frequencies available. The high-frequency relaxation exhibits an Arrhenius-like temperature dependence with an activation energy of (1.10 ± 0.05) eV (Fig. 6). Hence, it represents a noncooperative process. More detailed measurements above 120°C reveal an additional relaxation between the low- and the high-frequency relaxation ('intermediate-frequency' relaxation, Fig. 7). The low-frequency relaxation appears as a distinct loss maximum only at 180°C. As required by the Kramers–Kronig relation, it is accompanied by a 'step' in ε'. At lower temperatures, the low-frequency relaxation is hidden by a strong dispersion for which the frequency dependencies of the real part ε' and the imaginary part ε'' of the complex permittivity are almost perfectly parallel. Both, ε' and ε'' follow the same function, given by the power law $\sigma_{ac} \sim \omega^n$, where σ_{ac} is the ac conductivity. The exponent n was calculated as 0.32 ± 0.02 from the slope n − 1 of $\varepsilon'(\omega)$ or $\varepsilon''(\omega)$ or from the frequency-independent ratio $\varepsilon''/\varepsilon' \approx \chi''/\chi' = \cot(n\pi/2)$, where χ denotes the complex susceptibility. Parallel frequency dependences of ε' and ε'' are particularly well known for ionic conductors [21].

To obtain more information about the relaxation parameters of the observed relaxation regions, three Havriliak–Negami (HN) functions for the relaxation processes and a power law for the conductivity were fitted to the loss curve measured at 180°C (Fig. 8). The respective relaxation strengths $\Delta\varepsilon'$ obtained from the areas underneath the HN curves as well as the respective maximum dielectric losses ε''_{max} of the three relaxation regions are listed in Table 1. The frequency range of the low-frequency

Table 1
Maximum frequencies f_{max}, relaxation strengths $\Delta\varepsilon'$ and maximum dielectric losses ε''_{max} of dielectric relaxation processes in Az-PVA at 180°C as determined from the Havriliak–Negami fits

	f_{max}	$\Delta\varepsilon'$	ε''_{max}
Low-frequency relaxation	79 mHz	380	190
Intermediate-frequency relaxation	14 Hz	14	5.4
High-frequency relaxation	1.75 kHz	0.65	0.22

relaxation as well as the corresponding values of $\Delta\varepsilon'$ and ε''_{max} at 180°C cannot be explained with isolated or cooperative dipolar relaxations. The same is true for the intermediate-frequency relaxation. The present results indicate that these processes are related to charge carriers. It is remarkable that two current maxima also appear in the hysteresis curves, which probably correspond to the low-frequency and intermediate-frequency relaxations.

A distinct α relaxation which would indicate the onset of segmental main-chain motions, could not be detected. This confirms the DSC results. However, on the basis of the present findings, the observed relaxation regions cannot be unambiguously attributed to molecular mechanisms. Further studies are necessary in order to clarify the unusual dielectric behaviour.

4.5. Determination of the maximum possible pyroelectric coefficient from dielectric data

If dipole libration is neglected the experimental pyroelectric coefficient can be calculated from the dielectric data. This also allows a determination of the degree of orientation of the molecular dipoles.

Without dipole libration, the differentiation of Eq. (2) yields a relation between the experimental pyroelectric coefficient p_{exp} and the total frozen polarisation P [15]:

$$p_{exp} = \frac{\varepsilon_\infty + 2}{3}\alpha P \tag{4}$$

where $\alpha = (1/V) \times dV/dT$ is the coefficient of thermal volume expansion for a film that can expand freely. Eq. (4) has to be slightly modified if film expansion is restricted [5]. If the thermal expansion coefficient and the polarisation are known, the pyroelectric coefficient may be predicted.

The values of α and ε_∞ can be obtained from the temperature dependence of the dielectric susceptance at a sufficiently high frequency where all dipoles are immobile. In this case, the susceptance B, which is a function of the angular frequency ω, is given by:

$$B(\omega) = \omega\varepsilon_\infty\varepsilon_0\frac{A}{d} \tag{5}$$

where ε_0 is the permittivity of free space, A the electrode area, and d the film thickness. B is also a function of temperature. In the present case of a free-standing film clamped between two solid metal electrodes, the temperature dependence of B is given only by the temperature dependence of ε_∞. By means of the Clausius–Mossotti relation, $\varepsilon_\infty(T)$ can be related to the thermal expansion coefficient:

$$\frac{d\varepsilon_\infty}{dT} = \frac{(\varepsilon_\infty + 2)(\varepsilon_\infty - 1)}{3}\alpha \tag{6}$$

Differentiating B with respect to T and inserting $d\varepsilon_\infty/dT$ results in:

$$\frac{1}{B}\frac{dB}{dT} = \left[\frac{(\varepsilon_\infty + 2)(\varepsilon_\infty - 1)}{3\varepsilon_\infty}\right]\alpha \tag{7}$$

The values of B, dB/dT and ε_∞ are obtained from the experimental results. Thus, α may be calculated.

If the (low) crystallinity of the Az-PVA film is neglected, its maximum possible pyroelectric coefficient can be estimated as follows. The temperature dependence of the susceptance at a frequency of 1 kHz and for temperatures at which the low-, intermediate- and high-frequency relaxations are frozen is shown in Fig. 9. The expected linear dependence is superimposed with the small relaxation process mentioned at the beginning of the previous section. Nevertheless, the data can be fitted well with a straight line. From the slope $dB/dT = 3.28 \times 10^{-10}$ S K^{-1} of the regression line and from the values of $B = 3.39 \times 10^{-6}$ S at $T = 200$ K and of $\varepsilon_\infty = 1.79$, a volume thermal expansion coefficient of $\alpha = 1.73 \times 10^{-4}$ K^{-1} is obtained. Finally, on the basis of Eq. (4) with the theoretical polarisation at saturation, $P_S = 3.0 \times 10^{-2}$ C m^{-2}, a maximum possible pyroelectric coefficient of $p_{exp} = 6.6\ \mu$C (m^{2}K)$^{-1}$ is calculated. This is a typical value for amorphous glassy polymers.

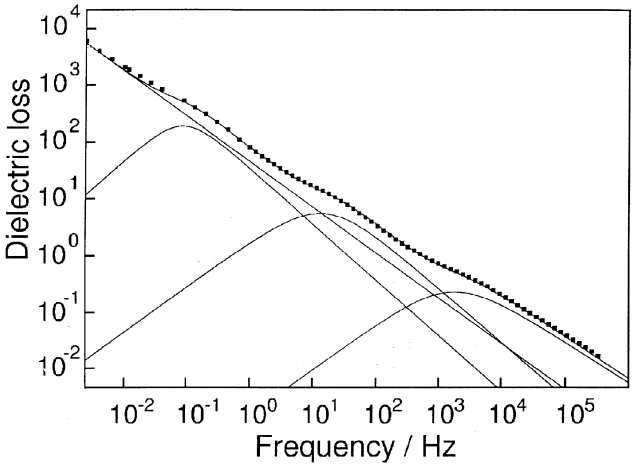

Fig. 8. Dielectric loss at 180°C (■) and Havriliak–Negami and conductivity fitting functions as well as their superposition (——).

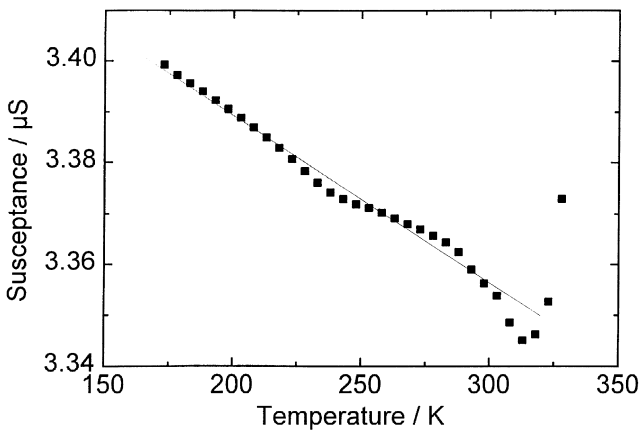

Fig. 9. Susceptance vs temperature at a frequency of 1 kHz in the low-temperature range: (■) and linear regression from 173 to 303 K, correlation factor 0.994 (——).

At a poling field of 75 MV m^{-1} a value of $p_{exp} = 1.5\ \mu C\ (m^2K)^{-1}$ is measured (cf. Fig. 3), which means that only 23% of the saturation polarisation are reached. This corresponds to an average tilt angle of $< \Theta > = 77°$. It can be concluded that the thermal poling was not very efficient. Unfortunately, higher fields were not possible because of electrical breakdown.

5. Conclusions

On the basis of all experimental results, it is suggested that the observed pyroelectric effect and the pronounced dielectric hysteresis must be attributed to different microscopic mechanisms in the sample material. The observed pyroelectricity indicates a field-induced orientation of the A-π-D dipoles. However, the observed pyroelectricity is essentially a secondary one because it is very unlikely that the A-π-D dipoles can librate during heating. The dipoles are relatively large and rigid. Their long aliphatic tails as well as the absence of a spacer between them and the main chain will hinder any separate movement of the polar group. The DSC results, as well as the absence of a clear α relaxation in the dielectric spectrum point towards a mainly amorphous material that remains in a glassy state up to the melting region. Because of these structural and thermal peculiarities, the observed low efficiency of the thermal poling and the reported high stability of the pyroelectric effect at room temperature can be expected.

The large polarisation found in the hysteresis measurements originates essentially from a displacement of charge carriers, probably ions, between internal phase boundaries. The most convincing argument for this interpretation comes from the comparison of the experimentally determined polarisation charge and the maximum theoretically possible dipolar polarisation, calculated under the assumption that the sample consists of just one macro-domain. The huge low-frequency permittivities also support this interpretation. The internal field of the polarisation charge partially compensates the externally applied field. This is probably the reason for the fact that pyroelectric coefficients at low applied fields were found to be smaller than expected from the Langevin function.

We can only speculate about the nature of the boundaries which cause the polarisation of charge carriers. The nearly linear behaviour of the conduction component in the current–voltage characteristics of Fig. 4 indicates that it is hardly influenced by space charges. This means that the deviation from a uniform charge distribution is not very large. Such a situation indicates a charge accumulation at boundaries between crystalline and amorphous regions rather than an electrode polarisation. Even if the crystallinity of the Az-PVA is low, there may be enough boundaries to cause a significant polarisation resulting from charge carriers if their concentration and mobility is sufficiently high.

It was already pointed out by Lines and Glass [7] that a charge-carrier polarisation in an inhomogeneous structure should also contribute to the pyroelectric effect because the thermal expansion coefficients of the crystalline and amorphous phases are different. Hence, the relative change of distance between trapped positive and negative charges during heating or cooling will differ from the change of the sample thickness. There are indications that the crystallinity of the sample material strongly depends on the conditions of preparation. Casted films which were dried slowly were not fully transparent. It will be an interesting topic for further research to study the dependence of the pyroelectric coefficient on crystallinity. This might lead to greater insight into the molecular processes that are causing the observed unusual electric and dielectric behaviour of Az-PVA.

The current–voltage dependences of Fig. 4, which implicitly include time, can easily be transformed into ferroelectric-like hysteresis curves by integration. On the other hand, if we define a ferroelectric as a polar material whose dipoles are intrinsic and can be reversed by application of a sufficiently large electric field, then ferroelectricity in this material is very unlikely for the above-mentioned reasons. Last, but not least, the present example demonstrates that a ferroelectric-like hysteresis is necessary, but by no means sufficient for true ferroelectricity.

Acknowledgements

The authors are indebted to Prof. Dr. S. Bauer (University of Linz, Austria) for stimulating discussions, to R. Dietel and Dr. G. Knochenhauer for valuable support, and to M. Ehlert, S. Meyerhöfer and J. Weingärtner for experimental assistance. The sample material was kindly provided by the Institute of Thin Film Technology and Microsensorics, Kantstrasse 55, D-14513 Teltow, Germany. Partial financial support from the Deutsche Forschungsgemeinschaft via the Graduiertenkolleg ‘Polymerwerkstoffe’ is gratefully acknowledged.

References

[1] Bauer S. Trends in Polymer Science 1995;3:288.
[2] Xiao DQ, Lang SB. IEEE Trans Electr Insul 1989;23:503.
[3] Coufal H, Mandelis A. Ferroelectrics 1991;118:379.
[4] Bauer S, Lang SB. IEEE Trans Dielectr Electr Insul 1996;3:647.
[5] Bauer S. J Appl Phys 1996;80:5531.
[6] Bauer S, Bauer-Gogonea S, Yilmaz S, Wirges W, Gerhard-Multhaupt R. In: Lindsay GA, Singer KD, editors. Polymers for second-order nonlinear optics. ACS Symposium Series. Washington, DC: American Chemical Society, 1995;201 304.
[7] Lines ME, Glass AM. Principles and applications of ferroelectrics and related materials. Oxford: Clarendon Press, 1977:549.
[8] Garn LE, Sharp EJ. J Appl Phys 1982;53:8974–8980.
[9] Carr PL, Davies GR, Ward IM. Polymer 1993;34:5.
[10] Davies GR, Hubbard HVSt A, Ward IM, Feast WJ, Gibson VC, Khosravi E, Marshall EL. Polymer 1995;36:235.
[11] Janietz D, Bauer M. Makromol Chem 1991;192:2635.

[12] Stewart JJP. J Comput Aided Mol Design 1990;4:1105.
[13] Frübing P, Weingärtner J, Brehmer L. Dielectrics Newsletter, Nov. 1997, p. 1; available from Novocontrol GmbH, Obererbacher Strasse 9, D-56414 Hundsangen, Germany.
[14] Wunderlich B. Macromolecular physics, vol. 3: Crystal melting. New York: Academic Press, 1980:69.
[15] Mopsik FI, Broadhurst MG. J Appl Phys 1975;46:4204.
[16] Brehmer L, Kaminorz Y, Grasnick G, Herkner H. Macromolecular Symposia 1996;102:391.
[17] Lide DR, editor. CRC handbook of chemistry and physics, 74th ed. 1993, Vol. 94, pp. 9–44.
[18] Janietz D. Personal communication.
[19] Fukada E, Tasaka S, Nalwa HS. In: Nalwa HS, editor. Ferroelectric polymers. New York: Marcel Dekker, 1995:378.
[20] Hattori T, Takahashi Y, Iijima M, Fukada E. J Appl Phys 1996;79:1713.
[21] Jonscher AK. Dielectric relaxation in solids. London: Chelsea Dielectric Press, 1983:224–234.